we observe sets of regulatory sites that exhibit patterns of coordinated regulation (e.g., *LYN*, encoding a tyrosine kinase involved in B cell signaling) (Fig. 4B), although reproducibility of these patterns across biological replicates was modest (fig. S22). Given the sparsity of the data, identifying pairs of coaccessible DNA elements within individual loci is statistically challenging and merits further development.

We report chromatin accessibility maps for >15,000 single cells. Our combinatorial cellular indexing scheme could feasibly be scaled to collect data from ~17,280 cells per experiment by using 384-by-384 barcoding and sorting 100 nuclei per well (assuming similar cell recovery and collision rates) (fig. S1) (*19*). Particularly as large-scale efforts to build a human cell atlas are contemplated (*23*), it is worth noting that because DNA is at uniform copy number, single-cell chromatin accessibility mapping may require far fewer reads per single cell to define cell types, relative to single-cell RNA-seq. As such, this method's simplicity and scalability may accelerate the characterization of complex tissues containing myriad cell types, as well as dynamic processes such as differentiation.

REFERENCES AND NOTES

1. A. B. Stergachis *et al.*, *Cell* **154**, 888–903 (2013).
2. R. E. Thurman *et al.*, *Nature* **489**, 75–82 (2012).
3. A. P. Boyle *et al.*, *Cell* **132**, 311–322 (2008).
4. J. D. Buenrostro, P. G. Giresi, L. C. Zaba, H. Y. Chang, W. J. Greenleaf, *Nat. Methods* **10**, 1213–1218 (2013).
5. N. Navin *et al.*, *Nature* **472**, 90–94 (2011).
6. A. R. Wu *et al.*, *Nat. Methods* **11**, 41–46 (2014).
7. D. A. Jaitin *et al.*, *Science* **343**, 776–779 (2014).
8. Q. Deng, D. Ramsköld, B. Reinius, R. Sandberg, *Science* **343**, 193–196 (2014).
9. A. K. Shalek *et al.*, *Nature* **498**, 236–240 (2013).
10. C. Trapnell *et al.*, *Nat. Biotechnol.* **32**, 381–386 (2014).
11. S. A. Smallwood *et al.*, *Nat. Methods* **11**, 817–820 (2014).
12. T. Nagano *et al.*, *Nature* **502**, 59–64 (2013).
13. J. Gole *et al.*, *Nat. Biotechnol.* **31**, 1126–1132 (2013).
14. H. C. Fan, G. K. Fu, S. P. A. Fodor, *Science* **347**, 1258367 (2015).
15. A.-E. Saliba, A. J. Westermann, S. A. Gorski, J. Vogel, *Nucleic Acids Res.* **42**, 8845–8860 (2014).
16. X. Pan, *Single Cell Biol.* **3**, 106 (2014).
17. A. Adey *et al.*, *Genome Res.* **24**, 2041–2049 (2014).
18. S. Amini *et al.*, *Nat. Genet.* **46**, 1343–1349 (2014).
19. Materials and methods are available as supplementary materials on *Science* Online.
20. A. Adey *et al.*, *Genome Biol.* **11**, R119 (2010).
21. F. Yang, T. Babak, J. Shendure, C. M. Disteche, *Genome Res.* **20**, 614–622 (2010).
22. The ENCODE Project Consortium, *Nature* **489**, 57–74 (2012).
23. A. Regev, The Human Cell Atlas; www.genome.gov/Multimedia/Slides/GSPFuture2014/10_Regev.pdf.

ACKNOWLEDGMENTS

We thank the Trapnell and Shendure laboratories, particularly R. Hause, C. Lee, V. Ramani, R. Qiu, Z. Duan, and J. Kitzman, for helpful discussions; D. Prunkard, J. Fredrickson, and L. Gitari in the Rabinovitch laboratory for their exceptional assistance in flow sorting; and C. Disteche for the Patski cell line. This work was funded by an NIH Director's Pioneer Award (1DP1HG007811 to J.S.) and a grant from the Paul G. Allen Family Foundation (J.S.). C.T. is supported in part by the Damon Runyon Cancer Research Foundation (DFS-#10-14). All sequencing data are available from the NIH National Center for Biotechnology Information Gene Expression Omnibus (accession number GSE68103). L.C., K.L.G., and F.J.S. declare competing financial interests in the form of stock ownership and paid employment by Illumina, Inc. One or more embodiments of one or more patents and patent applications filed by Illumina may encompass the methods, reagents, and data disclosed in this manuscript. All methods for making the transposase complexes are described in (*18*); however, Illumina will provide transposase complexes in response to reasonable requests from the scientific community subject to a material transfer agreement. Some work in this study is related to technology described in patent applications WO2014142850, 2014/0194324, 2010/0120098, 2011/0287435, 2013/0196860, and 2012/0208705.

SUPPLEMENTARY MATERIALS

www.sciencemag.org/content/348/6237/910/suppl/DC1
Materials and Methods
Figs. S1 to S22
Tables S1 and S2
References (*24*–*39*)

19 March 2015; accepted 24 April 2015
Published online 7 May 2015;
10.1126/science.aab1601

VIROLOGY

A virus that infects a hyperthermophile encapsidates A-form DNA

Frank DiMaio,[1]* Xiong Yu,[2]* Elena Rensen,[3] Mart Krupovic,[3] David Prangishvili,[3]† Edward H. Egelman[2]†

Extremophiles, microorganisms thriving in extreme environmental conditions, must have proteins and nucleic acids that are stable at extremes of temperature and pH. The nonenveloped, rod-shaped virus SIRV2 (*Sulfolobus islandicus* rod-shaped virus 2) infects the hyperthermophilic acidophile *Sulfolobus islandicus*, which lives at 80°C and pH 3. We have used cryo–electron microscopy to generate a three-dimensional reconstruction of the SIRV2 virion at ~4 angstrom resolution, which revealed a previously unknown form of virion organization. Although almost half of the capsid protein is unstructured in solution, this unstructured region folds in the virion into a single extended α helix that wraps around the DNA. The DNA is entirely in the A-form, which suggests a common mechanism with bacterial spores for protecting DNA in the most adverse environments.

Extreme geothermal environments, with temperatures above 80°C, are the habitat of hyperthermophilic DNA viruses that parasitize Archaea (*1*). These viruses have more than 92% of genes without homologs in databases (*2*, *3*), distinct protein folds (*4*), and distinct mechanisms of viral egress (*5*). The high diversity of virion morphotypes may underpin virion morphogenesis and DNA packaging, which could determine the high stability of the virions. Viruses from the family *Rudiviridae* (*6*) consist of a nonenveloped, helically arranged nucleoprotein composed of double-stranded DNA (dsDNA) and thousands of copies of a 134-residue protein. To understand the mechanisms stabilizing rudiviral DNA in natural habitats of host cells, which involve high temperatures (~80°C) and low pH values (~pH 3), we used cryo–electron microscopy (cryo-EM) to analyze the rudivirus SIRV2 (*Sulfolobus islandicus* rod-shaped virus 2) (*6*), which infects the hyperthermophilic acidophilic archaeon *Sulfolobus islandicus* (*7*) (see supplementary materials and methods). Members of the archaeal genus *Sulfolobus* maintain their cytoplasmic pH neutral at pH 5.6 to 6.5 (*8*, *9*). SIRV2 is therefore exposed to a wide range of pH values: from about pH 6 in the cellular cytoplasm, where it assembles and maturates (*10*), to pH 2 to 3 in the extracellular environment. We performed our studies at pH 6. SIRV2 is stable over a wide range of temperatures: from −80°C, the temperature at which the virus can be stored for years without loss of infectivity, to 80°C, the temperature of its natural environment. The overall morphology of the virion is maintained, regardless of the use of negative-stain imaging at 75°C (*11*) or cryo-EM with a sample at 4°C before vitrification (Fig. 1A).

Electron cryo-micrographs of SIRV2 (Fig. 1A) showed strong helical striations in most of the virions with a periodicity of 42 Å. We performed three-dimensional (3D) reconstruction using the iterative helical real space reconstruction method (*12*), after first determining the helical symmetry. Only one solution (with 14.67 subunits per turn of the 42 Å pitch helix) yielded a reconstruction with recognizable secondary structure, almost all α helical, and a resolution of ~3.8 Å in the more-ordered interior, which surrounds the DNA (fig. S2). The asymmetric unit was a symmetrical dimer, the α helices of which were wrapping around a continuous dsDNA. The DNA

[1]Department of Biochemistry, University of Washington, Seattle, WA 98195, USA. [2]Department of Biochemistry and Molecular Genetics, University of Virginia, Charlottesville, VA 22908, USA. [3]Institut Pasteur, Department of Microbiology, 25 rue du Dr. Roux, Paris 75015, France.
*These authors contributed equally to this work. **†Corresponding author. E-mail: egelman@virginia.edu (E.H.E.); david.prangishvili@pasteur.fr (D.P.)**

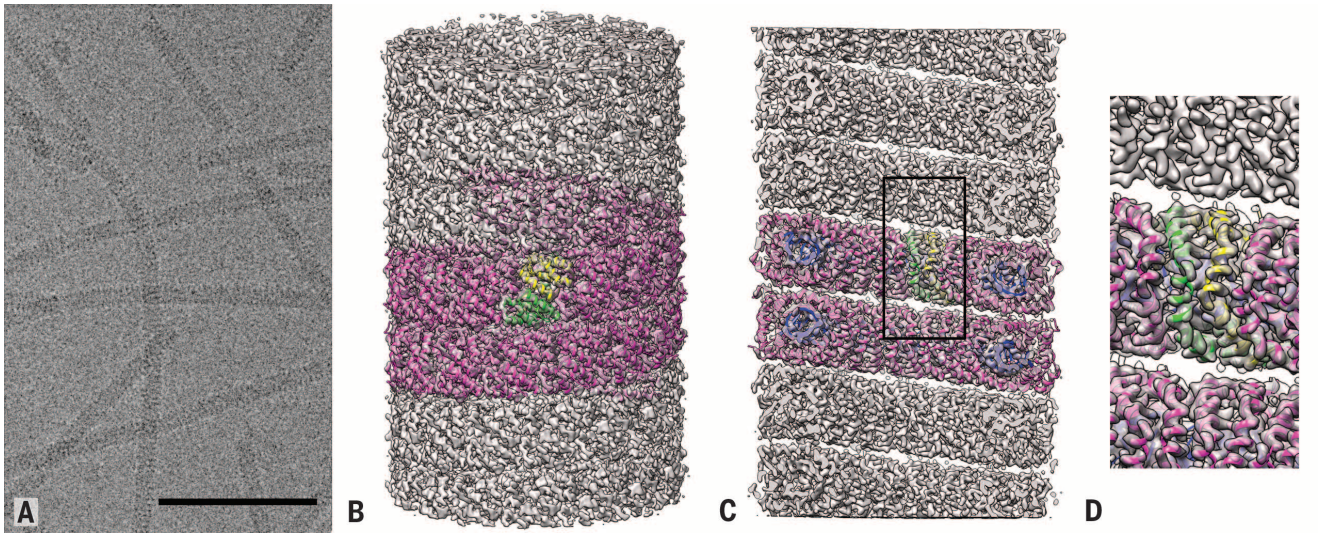

Fig. 1. Cryo-EM and 3D reconstruction of SIRV2. (**A**) Micrograph showing SIRV2 virions in vitreous ice. Scale bar, 1000 Å. (**B**) Side view of the reconstructed virion with a ribbon model for the protein (magenta). The asymmetric unit in the virion contains a protein dimer, and one is shown with one chain in yellow and the other in green. (**C**) Cutaway view showing the hollow lumen with the all α-helical protein segments that line the lumen. These α helices wrap around the dsDNA (blue) and encapsidate it. (**D**) Close-up view of the region shown within the rectangle in (C).

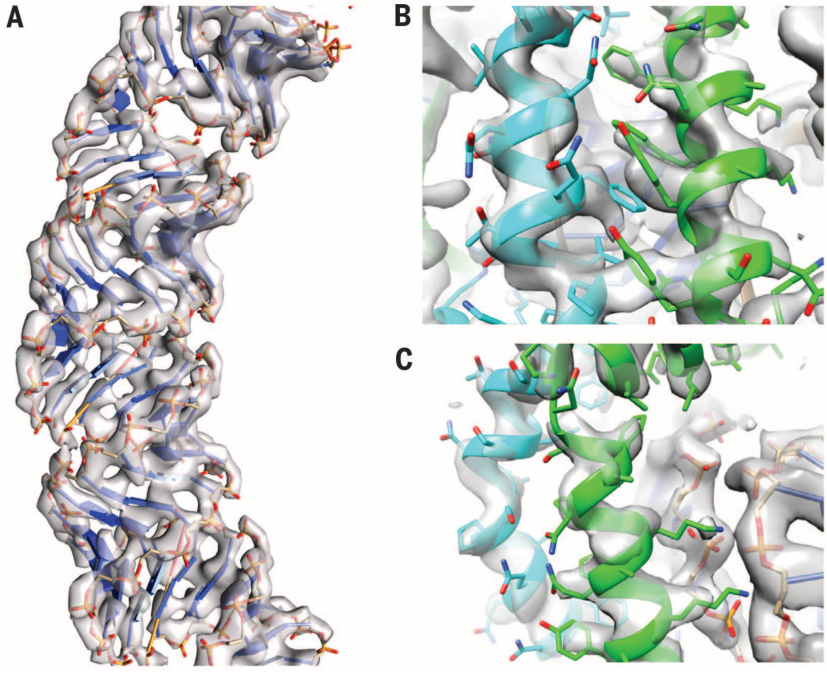

Fig. 2. The refined atomic model in the 3D reconstruction. (**A**) The density allows accurate tracing of the nucleotide chain. (**B**) The interface between helices within the asymmetric unit features large numbers of aromatic residues, which aid in correct registration of the sequence. (**C**) Side chains at the protein-DNA interface are well defined in density.

was in an A-form, in contrast to the B-form DNA (B-DNA) observed in icosahedral bacteriophages (*13*–*15*).

We used Rosetta guided by restraints from the EM data to determine and refine the atomic structure of SIRV2 (*16*). We began by docking a model of A-form DNA (A-DNA) into the map. The resulting model showed good agreement with the experimental data, where the rigid phosphate groups were well defined (Fig. 2, A and C). A dimeric crystal structure from a close homolog with 88% identity [Protein Data Bank identifier (PDB ID) 3F2E] was docked into the map. However, this model lacked 51 N-terminal residues, the first 46 of which were shown by nuclear magnetic resonance (NMR) to be unstructured in the monomer in solution and not part of the fragment crystallized (*17*). In the cryo-EM reconstruction, these residues formed helices wrapping around the DNA. Because the NMR studies were done at pH 6, the same pH used for our cryo-EM studies, the gain in structure of these residues is associated with assembly rather than a change in pH. We used RosettaCM (*18*) to build these N-terminal residues into the density map. A representative model was chosen from a well-converged, low-energy ensemble (fig. S4); this model shows good agreement with the side-chain density in the map at both protein-protein interfaces (Fig. 2B) and protein-DNA interfaces (Fig. 2C). Seven N-terminal residues could not be placed in the density.

The final structure reveals that the N-terminal residues form a helix-turn-helix motif encapsulating the A-DNA, with helices from each subunit in the asymmetric unit packing in an antiparallel configuration (Fig. 3, A and B). Proline residues in this region (Pro^{27}, Pro^{39}, and Pro^{50}) allow some helical deformation to tightly wrap the DNA. These interdigitated helices form a solvent-inaccessible surface surrounding the DNA (Fig. 3C). The DNA was confirmed as A-form (*19*), where the parameters [including an average base pair inclination of 25°, a negative slide (average = –1.6), and a negative x-displacement (average = –4.8)] match A-DNA, whereas the slide and x-displacement are positive for B-DNA. The average phosphate-phosphate distance along the DNA backbone is 5.9 Å, as opposed to ~7.0 Å for B-DNA. The diameter of the DNA is ~24 Å. At this resolution, the sugar pucker is not discernable. A slight bulge in the DNA occurs near the dimer interface, where a buried arginine side chain (Arg^{73}) interacts with one of the DNA phosphate groups, leading to some local deviations from A-DNA. Model bias was tested by starting with the B-form, which converged to the same final model (fig. S5). The DNA (Fig. 3D), whose axis is at a helical radius of ~60 Å, has three right-handed superhelical turns every 44 (= 3 × 14.67) repeats (turns) of the DNA. So there are 528 base pairs

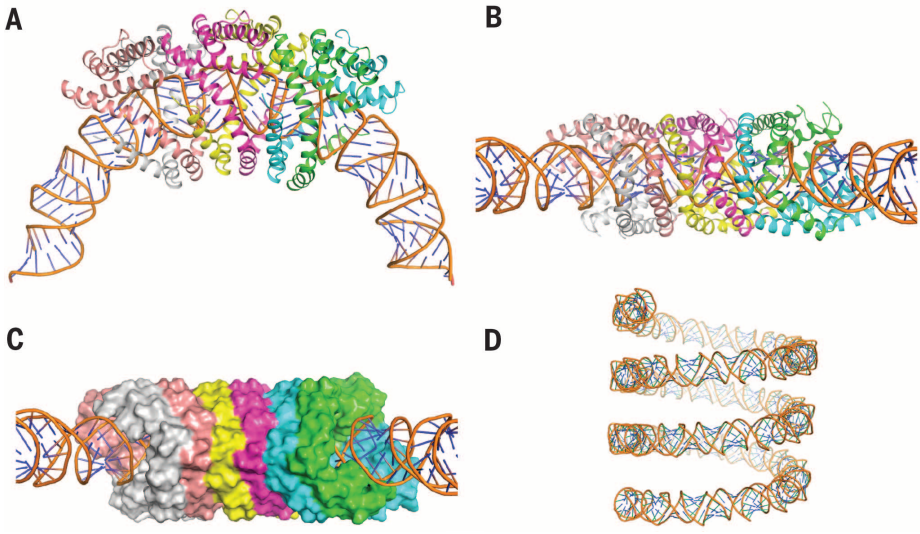

Fig. 3. The SIRV2 protein dimer helices fully encapsulate the DNA. (**A**) Three asymmetric units of the virion are shown, illustrating how the N-terminal helices wrap around the DNA, forming antiparallel helix-helix packing. (**B**) Side view. (**C**) Surface view of the protein (using a 1.4 Å probe radius). (**D**) The right-handed solenoidal supercoiling of the DNA, with three turns shown.

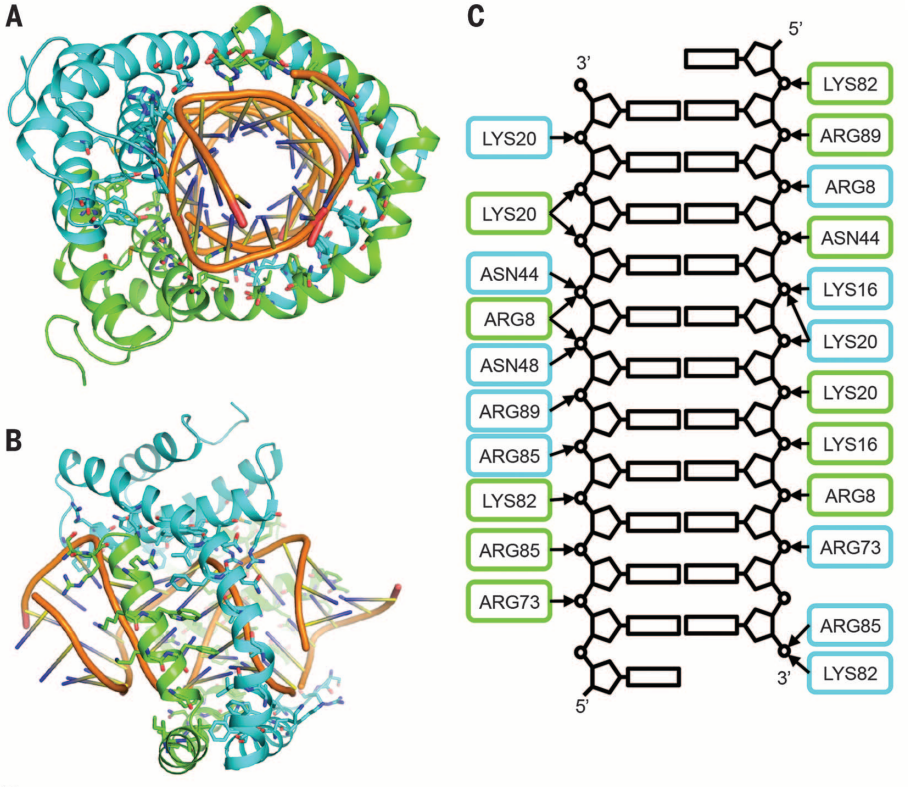

D

```
                10        20        40        50        70        80        90
SIRV2   MAKGHTSRSYSQRYAKWQAKFNA … VAQQNFQTNVPKF … GPNRAIYQGFGLKVARALNRIGS
SIRV1   MAKGHTKRSYSQRYAKWQAKFNA … VAQQNFQTNVPTF … GPNRAIYQGFGLKIARALNRIGS
ARV1    MAKGHTPRSYSQRYSKWSGKFTA … IAQENFQTNVPKF … GPSRAIYQGFGLKVERALNRIGS
SRV     MAKGRTPRSFTQRYAKWNAKFTA … IAQQNFQTNVPKF … GPNRAIYQGYALKVARALNRLGG
SMRV1   MAKGHTPRSFAQRYGKWQAKFTA … VAQGNFEQNSSLM … GPNRVIYQGFALKLYRAKNRIGN
```

Fig. 4. Overview of protein-DNA contacts in the virion. (**A**) The protein-DNA interface is mainly polar, with largely Arg and Lys side chains contacting phosphate groups in the DNA. (**B**) Side view. (**C**) Schematic indicating all of the polar protein-DNA contacts. The coloring of each subunit is the same as in (A) and (B). (**D**) A multiple sequence alignment with related archaeal rod-shaped viruses indicates that all of these contacts are well conserved (*29*). SIRV2, *Sulfolobus islandicus* rod-shaped virus 2; ARV1, *Acidianus* rod-shaped virus 1; SRV, *Stygiolobus* rod-shaped virus; SMRV1, *Sulfolobales* Mexican rudivirus 1. The yellow boxes indicate the residues that are interacting with the DNA backbones.

(= 44 × 12) per 47 right-handed turns, which yields an overall twist of 11.2 base pairs per turn (Fig. 3D).

DNA-protein contacts (Fig. 4, A to C) are largely polar, with nine conserved side chains (Arg^{8}, Lys^{16}, Lys^{20}, Asn^{44}, Asn^{48}, Arg^{73}, Lys^{82}, Arg^{85}, and Arg^{89}) directly interacting with the DNA phosphate groups. Additionally, the backbone of Ser^{9} makes contact with the phosphate backbone of the DNA. There are also several hydrophobic contacts with the DNA, most notably the aromatic residues Trp^{17}, Phe^{21}, Phe^{24}, and Phe^{52}, as well as Val^{37}. All of these residues are conserved in related rudiviruses (Fig. 4D), suggesting a similar method of DNA stabilization and protection. Extensive protein-DNA interactions in SIRV2 virions alleviate the necessity to package charge-neutralizing counterions (*13*, *14*). Within the dimer, protein-protein interfaces are largely hydrophobic. The interface is extensive, comprising ~17% of each monomer's surface area, with a total interface area of 1491 $Å^2$. Five aromatic residues (Tyr^{10}, Tyr^{14}, Trp^{17}, Phe^{21}, and Phe^{45}) form a well-packed barrier separating DNA from solvent. The protein-protein interface between adjacent dimers also forms a largely hydrophobic interface, with 1706 $Å^2$ of contact area between dimers on both sides. Interactions between dimers across the groove of the helix are weak and largely polar.

Small acid-soluble proteins (SASPs) are responsible for protecting DNA in Gram-positive bacterial spores (*20*) and are largely unstructured in solution (*21*–*24*), but they become α helical upon binding dsDNA (*25*, *26*). Almost half of the SIRV2 capsid protein is unstructured in solution (*17*), and this portion becomes α helical when bound to DNA in the virion. The binding of SASPs to DNA is saturable, with saturation occurring at an SASP:DNA weight ratio of ~3:1 (*27*). In the SIRV2 virion, we have now shown that the weight ratio of capsid protein to DNA is 3.5:1. The binding of the SASPs to DNA induces a dimerization of the SASPs (*25*), and the asymmetric unit in the virion contains a symmetrical dimer of the coat protein. The binding of SASPs to DNA induces

a transition from B-DNA to A-DNA (*27*), and an en masse transition of DNA from B-form to A-form can be induced in bacterial cells, suggesting that the A-form plays an unrecognized role in stabilizing DNA under adverse conditions such as dessication (*28*). Sequence analysis and structural comparison (with PDB ID 2Z3X) do not show obvious homology, suggesting that these similarities could have arisen as a result of convergent evolution.

REFERENCES AND NOTES

1. D. Prangishvili, *Annu. Rev. Microbiol.* **67**, 565–585 (2013).
2. D. Prangishvili, R. A. Garrett, E. V. Koonin, *Virus Res.* **117**, 52–67 (2006).
3. M. Krupovic, D. Prangishvili, R. W. Hendrix, D. H. Bamford, *Microbiol. Mol. Biol. Rev.* **75**, 610–635 (2011).
4. M. Krupovic, M. F. White, P. Forterre, D. Prangishvili, *Adv. Virus Res.* **82**, 33–62 (2012).
5. D. Prangishvili, T. E. Quax, *Curr. Opin. Microbiol.* **14**, 315–320 (2011).
6. D. Prangishvili *et al.*, *Genetics* **152**, 1387–1396 (1999).
7. C. Jaubert *et al.*, *Open Biol.* **3**, 130010 (2013).
8. M. Lübben, G. Schäfer, *J. Bacteriol.* **171**, 6106–6116 (1989).
9. C. Baker-Austin, M. Dopson, *Trends Microbiol.* **15**, 165–171 (2007).
10. A. Bize *et al.*, *Proc. Natl. Acad. Sci. U.S.A.* **106**, 11306–11311 (2009).
11. E. R. Quemin *et al.*, *J. Virol.* **87**, 13379–13385 (2013).
12. E. H. Egelman, *Ultramicroscopy* **85**, 225–234 (2000).
13. T. Y. Yu, J. Schaefer, *J. Mol. Biol.* **382**, 1031–1042 (2008).
14. S. A. Overman *et al.*, *Biospectroscopy* **4** (suppl.), S47–S56 (1998).
15. W. Earnshaw, S. Casjens, S. C. Harrison, *J. Mol. Biol.* **104**, 387–410 (1976).
16. F. S. DiMaio *et al.*, *Nat. Methods*, **12**, 361–365 (2015).
17. B. R. Szymczyna *et al.*, *Structure* **17**, 499–507 (2009).
18. Y. Song *et al.*, *Structure* **21**, 1735–1742 (2013).
19. X. J. Lu, W. K. Olson, *Nucleic Acids Res.* **31**, 5108–5121 (2003).
20. P. Setlow, *Trends Microbiol.* **15**, 172–180 (2007).
21. B. Setlow, P. Setlow, *J. Bacteriol.* **177**, 4149–4151 (1995).
22. C. S. Hayes, P. Setlow, *J. Bacteriol.* **179**, 6020–6027 (1997).
23. C. S. Hayes, B. Illades-Aguiar, L. Casillas-Martinez, P. Setlow, *J. Bacteriol.* **180**, 2694–2700 (1998).
24. C. S. Hayes, E. Alarcon-Hernandez, P. Setlow, *J. Biol. Chem.* **276**, 2267–2275 (2001).
25. C. S. Hayes, Z. Y. Peng, P. Setlow, *J. Biol. Chem.* **275**, 35040–35050 (2000).
26. K. S. Lee, D. Bumbaca, J. Kosman, P. Setlow, M. J. Jedrzejas, *Proc. Natl. Acad. Sci. U.S.A.* **105**, 2806–2811 (2008).
27. S. C. Mohr, N. V. Sokolov, C. M. He, P. Setlow, *Proc. Natl. Acad. Sci. U.S.A.* **88**, 77–81 (1991).
28. D. R. Whelan *et al.*, *J. R. Soc. Interface* **11**, 20140454 (2014).
29. Single-letter abbreviations for the amino acid residues are as follows: A, Ala; C, Cys; D, Asp; E, Glu; F, Phe; G, Gly; H, His; I, Ile; K, Lys; L, Leu; M, Met; N, Asn; P, Pro; Q, Gln; R, Arg; S, Ser; T, Thr; V, Val; W, Trp; and Y, Tyr.

ACKNOWLEDGMENTS

This work was supported by NIH grant GM035269 (to E.H.E.). The map and model have been deposited in the Electron Microscopy Data Bank (accession number EMD-6310) and in PDB (ID 3J9X), respectively. We thank K. Dryden for assistance with the microscopy.

SUPPLEMENTARY MATERIALS

www.sciencemag.org/content/348/6237/914/suppl/DC1
Materials and Methods
Figs. S1 to S5
References (*30*–*37*)

3 December 2014; accepted 21 April 2015
10.1126/science.aaa4181

RNA STRUCTURE

Structure of the HIV-1 RNA packaging signal

Sarah C. Keane,[1] Xiao Heng,[1]* Kun Lu,[1]† Siarhei Kharytonchyk,[2] Venkateswaran Ramakrishnan,[1] Gregory Carter,[1] Shawn Barton,[1] Azra Hosic,[1] Alyssa Florwick,[1] Justin Santos,[1] Nicholas C. Bolden,[1] Sayo McCowin,[1] David A. Case,[3] Bruce A. Johnson,[4] Marco Salemi,[5] Alice Telesnitsky,[2]‡ Michael F. Summers[1]‡

The 5′ leader of the HIV-1 genome contains conserved elements that direct selective packaging of the unspliced, dimeric viral RNA into assembling particles. By using a ^{2}H-edited nuclear magnetic resonance (NMR) approach, we determined the structure of a 155-nucleotide region of the leader that is independently capable of directing packaging (core encapsidation signal; Ψ^{CES}). The RNA adopts an unexpected tandem three-way junction structure, in which residues of the major splice donor and translation initiation sites are sequestered by long-range base pairing and guanosines essential for both packaging and high-affinity binding to the cognate Gag protein are exposed in helical junctions. The structure reveals how translation is attenuated, Gag binding promoted, and unspliced dimeric genomes selected, by the RNA conformer that directs packaging.

Assembly of HIV-1 particles is initiated by the cytoplasmic trafficking of two copies of the viral genome and a small number of viral Gag proteins to assembly sites on the plasma membrane (*1*–*6*). Unspliced, dimeric genomes are efficiently selected for packaging from a cellular milieu that includes a substantial excess of nonviral messenger RNAs (mRNAs) and more than 40 spliced viral mRNAs (*7*, *8*). RNA signals that direct packaging are located primarily within the 5′ leader of the genome and are recognized by the nucleocapsid (NC) domains of Gag (*4*). Transcriptional activation, splicing, and translation initiation are also dependent on elements within the 5′ leader, the most conserved region of the genome (*9*), and there is evidence that these and other activities are temporally modulated by dimerization-dependent exposure of functional signals (*6*, *10*–*13*).

Understanding the RNA structures and mechanisms that regulate HIV-1 5′ leader function has its basis in phylogenetic, biochemical, nucleotide reactivity, and mutagenesis studies (*4*). The dimeric leader selected for packaging appears to adopt a highly branched secondary structure, in which there are structurally discrete hairpins and helices that promote transcriptional activation (TAR), transfer RNA (tRNA) primer binding (PBS), packaging (ψ), dimer initiation (DIS), splicing (SD), and dimer stability (U5:AUG) (*4*, *14*) (Fig. 1). Although nuclear magnetic resonance (NMR) signals diagnostic of TAR, PBS, ψ, DIS, U5:AUG, and polyadenylate [poly(A)] helices have been observed in spectra obtained for the full-length dimeric leader (*13*, *15*) (Fig. 1A), signals diagnostic of a putative SD hairpin have not been detected (colored magenta in Fig. 1A) (*15*), and there is little agreement among more than 20 different structure predictions for residues adjacent to the helices (*4*). For example, predictions vary for stretches of residues shown by in vivo nucleotide reactivity (*16*) and cross-linking with immunoprecipitation (*17*) to reside at or near sites of Gag binding (*4*). The TAR, poly(A), and PBS hairpins of the HIV-1 leader are not required for efficient encapsidation (*15*), and a minimal HIV-1 packaging element, the core encapsidation signal (Ψ^{CES}), exhibits NC binding properties and NMR spectral features similar to those of the intact 5′ leader and is independently capable of directing vector RNAs into viruslike particles (*15*). To gain insights into the mechanism of HIV-1 genome selection, we determined the structure of Ψ^{CES} by NMR.

Contributions of slow molecular rotational motion to NMR relaxation were minimized by substituting the dimer-promoting GC-rich loop of the Ψ^{CES} DIS hairpin by a GAGA tetraloop (Fig. 1A). This prevented dimerization (Fig. 1B) but did not affect NC binding (Fig. 1C) or nuclear Overhauser effect spectroscopy (NOESY) NMR spectral patterns (*18*), indicating that the modified RNA retains

[1]Howard Hughes Medical Institute (HHMI) and Department of Chemistry and Biochemistry, University of Maryland Baltimore County (UMBC), 1000 Hilltop Circle, Baltimore, MD 21250, USA. [2]Department of Microbiology and Immunology, University of Michigan Medical School, Ann Arbor, MI 48109-5620, USA. [3]Department of Chemistry and Chemical Biology, Rutgers University, Piscataway, NJ 08854, USA. [4]One Moon Scientific, Incorporated, 839 Grant Avenue, Westfield, NJ 07090, USA, and City University of New York (CUNY) Advanced Science Research Center, 85 St. Nicholas Terrace, New York, NY 10031, USA. [5]Department of Pathology, Immunology, and Laboratory Medicine, College of Medicine, and Emerging Pathogens Institute, University of Florida, Gainesville, FL 32610, USA.
*Present address: Department of Biochemistry, University of Missouri, Columbia, MO 65211, USA. †Present address: Regeneron Pharmaceuticals, Incorporated, 777 Old Saw Mill River Road, Tarrytown, NY 10591, USA. **‡Corresponding author. E-mail: summers@hhmi.umbc.edu (M.F.S.); ateles@umich.edu (A.T.)**